Investigation of Guided-Particle Transport for Noninvasive Healing of Damaged Piping Systems by Use of Electro-Magneto-Mechanical Methods

Debanjan Mukherjee, Zeyad Zaky, and **Tarek I. Zohdi,** University of California, Berkeley; and **Amgad Salama** and **Shuyu Sun,** King Abdullah University of Science and Technology

Summary

Virtually all engineering applications involve the use of piping, conduits, and channels. In the petroleum industry, piping systems are extensively used in upstream and downstream processes. These piping systems often carry fluids that are corrosive, which leads to wear, cavitation, and cracking. The replacement of damaged piping systems can be quite expensive, both in terms of capital costs and in operational downtime. This motivates the present research on noninvasive healing of cracked piping systems. In this investigation, we propose to develop computational models for characterizing noninvasive repair strategies involving electromagnetically guided particles. The objective is to heal industrial-piping systems noninvasively, from the exterior of the system, during operation, resulting in no downtime and minimal relative cost. The particle accumulation at a target location is controlled by external electromagnetic/mechanical means. There are two primary effects that play a role for guiding the particles to the solid-fluid-interface/wall: mechanical shear caused by the fluid flow, and an electrical or magnetic force. In this work we develop and study a relationship that characterizes contributions of both, and ascertain how this relationship scales with characteristic physical parameters. Characteristic nondimensional parameters that describe system behavior are derived, and their role in design is illustrated. A detailed, fully 3D discrete-element-simulation framework is presented, and illustrated by use of a model problem of magnetically guided particles. The detailed particle behavior is considered to be regulated by three effects: the field strength, the mass-flow rate, and the wall interactions.

Introduction

Noninvasive healing of damaged piping systems can provide a solution to pipe repair in the field. In many industries, especially the petroleum industry, there is an extensive use of piping systems. According to the US Department of Transportation Pipeline and Hazardous Materials Safety Administration, more than 350,000 miles pipelines transporting natural gas, crude oil, and petroleum products are used daily (DOT 2014). These systems are run for long times without stoppage, naturally bringing about degradation. Stopping operation of these systems for repair can prove to be very costly. Not only is the opportunity for financial gains lost because of work stoppage, but there are also costs associated with repair of the damaged piping component(s). The motivation is then to investigate a noninvasive pipe-healing technique. By placing ferromagnetic or charged particles into a fluid flow and applying an external field, the desired effect is to attract the particles to the damage location and physically fuse them there by means of either chemical-reaction processes, laser sintering, heat pulse, or some other thermal/mechanical means. This noninvasive process can prove to be a cost-effective and low-downtime method.

This paper (SPE 169639) was accepted for presentation at the SPE International Oilfield Corrosion Conference and Exhibition, Aberdeen, 12–13 May 2014, and revised for publication. Original manuscript received for review 9 February 2014. Revised manuscript received for review 18 December 2014. Paper peer approved 24 December 2014.

Magnetically controlled suspensions, with an emphasis on hydrodynamics-application design, have been investigated by Odenbach (2003). This research is concerned with altering the fluid properties by applying an external field. Magnetically guiding particles is also of interest in microscale-device applications. A microfluidic pump that uses magnetic actuation to push a ferrofluid through a microchannel was investigated by Hatch and Kamholz (2001). The particles used in this application were on the nanoscale. In the medical field, guiding particles to target cells by use of external fields is of interest. Peasley (1996) investigated destruction of HIV-infected cells by ferrofluid particles manipulated by an external magnetic field. Similarly, Jordan et al. 1999) investigated treating cancer cells by use of an alternating-current magnetic field. Although the common theme of guiding particles with an external field exists, the current study is not concerned with resulting fluid properties or targeting undesirable cells. This work is interested in guiding particles in a fluid flow to a damage site and repairing it.

The problem of noninvasive healing can be subdivided into two distinct processes. Of primary interest is to attract the particles to the damaged location of the pipe. Thereafter, a process of physically fusing the particles into place is needed. Because the process is governed by many physical parameters, a design space is needed. Nondimensionalization of the governing particle-dynamics equation was therefore carried out. More details and results from this process are shown in later sections of this study. For the modeling, a 3D discrete-element framework is presented and used to simulate the process. A critical benefit to the present framework is flexibility; it allows for various configurations to be examined.

The study begins by explaining the proposed noninvasive healing technique. Forces acting on an isolated particle are then discussed, with models for fluid/particle interaction, magnetic particles in a magnetic field, and charged particles in an electromagnetic field. A parametric model for the design space is then discussed, with a focus on addressing the competition between the fluid/particle interaction and interaction with electromagnetic fields. Implications for design and numerical examples are illustrated. Thereafter, a 3D discrete-element-simulation framework is discussed with a focus on the flow-velocity profile, particle/particle-contact interactions, particle interactions with a pipe wall, and a solution algorithm for system dynamics. The implementation of the framework is then illustrated with a model problem of magnetically guided ferromagnetic-particle streams.

Proposed Noninvasive Healing Technique

The proposed method for noninvasive healing is centered on the idea of releasing ferromagnetic or charged particles into a fluid flow within an internal channel or pipe. Externally applied electromagnetic fields can be used to guide these particles toward a particular location of interest, which is the location of damage. The strategy involves guiding these particles and accumulating them at the damage site, followed by a physical manipulation of the particles to repair the damage (e.g., fusion, chemical reaction).

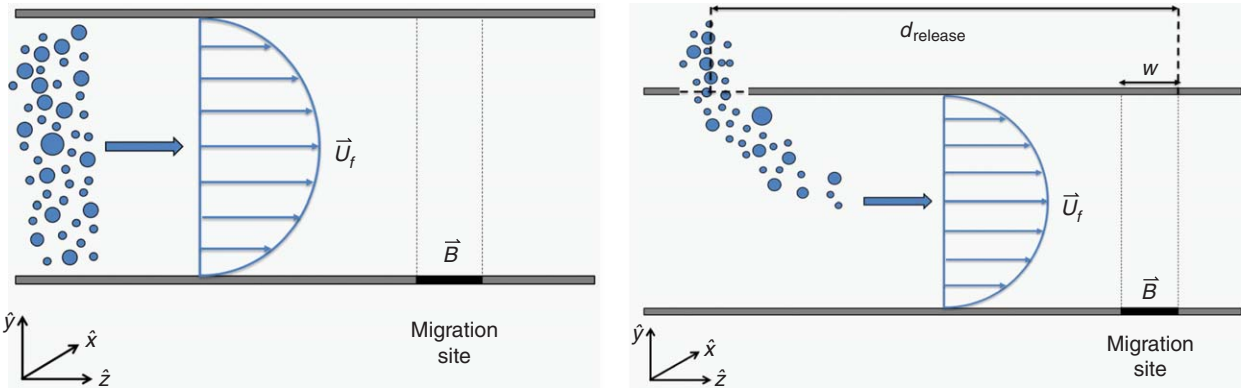

Fig. 1—Schematic of the proposed strategy for healing an internal crack/wear within the pipe, by use of particles guided to the repair site by means of externally applied electromagnetic fields. (a) Particles introduced from a pipe inlet. (b) Particles introduced from a pipe orifice.

As shown in **Fig. 1,** the conceptual visualization of the process can be represented in two different forms schematically. In Fig. 1a, particles are released at a certain cross-sectional location into the pipe flow, whereas in Fig. 1b, they are injected from an orifice along the pipe wall. It is anticipated that one or the other may be advantageous to real-life applications and that the particle behavior would differ on the basis of the mechanism of release. To illustrate the simulation framework, the configuration of Fig. 1a has been used; however, the physical principles remain the same for both. The possible variabilities in particle size have also been indicated in Fig. 1, in terms of illustrating the particles to be polydisperse.

Forces Acting on an Isolated Particle

Fluid/Particle Interaction. The fluid/particle interactions will be assumed to be one-way coupled. This entails the assumption that the particles do not affect the fluid flow significantly. For the applications desired, the particle sizes will be small and hence lead to low particle-response times, making this a reasonably good approximation. A fully resolved solution of the flow around a sphere is a computationally intensive task, and is not required for the scope of the paper. Alternative approaches to characterizing the unsteady motion of the spherical particle in a fluid can be provided through an equivalent motion equation for the sphere obtained by superposing the steady and unsteady forces caused by the fluid on the particle. The most famous form of this was provided in Maxey and Riley (1983), and several modified versions of the same have been discussed in Berlemont et al. (1990), Mei (1994), Mei and Adrian (1992), and Kim et al. (1998). It is noted, however, that the drag force can be seen to be the most-dominant interaction that is present in a broad range of applications. For the scope of the current work, a correct estimation of the drag force will be a reasonable approximation, with the knowledge that more-involved forms of the forces can be resolved by use of the equations mentioned herein. By use of the standard form of the drag force,

$$\mathbf{F}_{\text{drag}} = \frac{1}{2}\rho_f C_D A(\mathbf{u}-\mathbf{v})\|\mathbf{u}-\mathbf{v}\|, \quad \ldots\ldots\ldots\ldots\ldots (1)$$

where ρ_f is the fluid density, A is the flow cross-sectional area, $\mathbf{u}$ is the fluid velocity, and $\mathbf{v}$ is the particle velocity. This would then require a reasonably accurate estimate of the drag coefficient $C_D(Re_p)$. There are numerous correlations available in the existing literature, including Crowe et al. (2011), Fritsching (2004), and Bailey and Hiatt (1972), among others. Of these, the correlation presented by Haider and Levenspiel (1989) finds applicability over a broad range of Reynolds numbers, and also has a very-low mean square error compared with values of drag coefficients obtained from available experimental data; hence, this will be the choice for modeling the pipe-healing system. Their correlation can be numerically expressed as

$$C_D(Re_p) = \frac{24}{Re_p}(1+0.1806Re_p^{0.6459}) + \frac{0.4251}{\left(1+\frac{6880.95}{Re_p}\right)}. \quad \ldots\ldots\ldots\ldots\ldots\ldots (2)$$

Magnetic Particles in a Magnetic Field. A plane current loop of sufficiently small size is referred to as an elementary current loop, and its behavior is described by use of the magnetic moment $\mu_m = IS\mathbf{n}$, where I is the current carried by the loop, S is the area bound by the loop, and vector $\mathbf{n}$ is the normal to the surface bounded by the loop. By use of Ampere's law on this elementary loop, the total potential energy U_{mag} and force of interaction $\mathbf{F}_{\text{mag}}$ of an elementary loop with a nonuniform magnetic field $\mathbf{B}$ can be given by

$$U_{\text{mag}} = -\boldsymbol{\mu}_m \cdot \mathbf{B}, \;\; \mathbf{F}_{\text{mag}} = \nabla(\boldsymbol{\mu}_m \cdot \mathbf{B}). \quad \ldots\ldots\ldots\ldots (3)$$

For a material, the magnetization vector $\mathbf{M}$ is defined to be the density of all the vector magnetic moments in a magnetic material at a given point, and mathematically is represented as

$$\mathbf{M} = \frac{\sum_{\delta V}\boldsymbol{\mu}_m}{\delta \mathcal{V}}. \quad \ldots\ldots\ldots\ldots\ldots\ldots\ldots\ldots (4)$$

The presence and orientation of these elementary magnetic moments in a material govern the material bulk behavior in the presence of a magnetic field. For example, diamagnetic materials are such that in the absence of an external magnetic field, there are no magnetic moments at the molecular level.

The magnetic-field intensity $\mathbf{H}$ is defined as $\mathbf{H} = \mathbf{B}/\mu_0 - \mathbf{M}$. For most materials, the magnetization vector can be assumed to be a linear function of the local magnetic-field vector $\mathbf{B}$, and the relationship is defined in terms of the magnetic susceptibility χ_m as $\mathbf{M} = \chi_m \mathbf{H}$. By use of these definitions, we can write

$$\mathbf{B} = \;\mu_0(1+\chi_m)\mathbf{H} = \mu_0\mu_r\mathbf{H} = \mu\mathbf{H}, \quad \ldots\ldots\ldots\ldots (5)$$

where μ_0 is the absolute permeability, μ_r is the relative magnetic permeability of the material, and μ is the magnetic permeability of the material. For a particle that is small in size (relative to the other dominant length scales of the system), the total magnetic moment can be given as a sum over the particle volume as $\sum \mu_m = \mathbf{M}\mathcal{V}_p$.

For paramagnetic and ferromagnetic particles, it can be assumed that all the magnetic dipoles in the material are oriented

along the direction of **B**, following which, by use of Eq. 3, the expression for the force can be obtained,

$$\mathbf{F}_{\text{mag}} = \nabla(\mathbf{M}\mathcal{V}_p \cdot \mathbf{B}) = \nabla\left(\frac{\mathcal{V}_p \chi_m}{\mu_0 \mu_r}\mathbf{B}\cdot\mathbf{B}\right), \quad \ldots\ldots\ldots\ldots (6)$$

where the definitions of susceptibility and permeability have been used to relate the force entirely to the applied external magnetic field **B**.

Charged Particles in an Electromagnetic Field. For a charged particle in an applied electromagnetic field, the force of interaction is given by use of the classical Lorentz force. For applied electric field of strength **E** and applied magnetic field of strength **B**, the force of interaction is

$$\mathbf{F}_{em} = q(\mathbf{E} + \mathbf{v}\times\mathbf{B}). \quad \ldots\ldots\ldots\ldots\ldots\ldots\ldots (7)$$

Parametric Model for the Design Space for Guided Particulate Streams

We address now the issue of constructing a model for the design space to guide the selection of the major parameters for setting up a pipe-healing strategy using electromagnetically guided particles. The primary design parameters of interest would be the particle sizes, the particle charge, the applied-field strengths, and the flow velocities of the pipe fluid. As the particles move in the fluid, the forces caused by the applied fields and those caused by the surrounding fluid actually compete with each other in determining whether the particles migrate efficiently to the target site for repair. Through simple physical considerations, the effect of this competition in terms of parameter selection will be illustrated.

Magnetic Particle in a Magnetic Field. The motion of a particle in a generalized fluid volume under the action of an externally applied magnetic field is considered here. Expressing the total fluid forces on the particle as $\mathbf{F}_{fl}$ and the interaction forces from the magnetic field as $\mathbf{F}_{\text{mag}}$, the motion equation is given by

$$m_p\frac{d\mathbf{v}}{dt} = \mathbf{F}_{fl} + \mathbf{F}_{\text{mag}}. \quad \ldots\ldots\ldots\ldots\ldots\ldots\ldots (8)$$

By use of the expressions for the forces outlined in the preceding section, this motion equation can be written in complete detail as

$$m_p\frac{d\mathbf{v}}{dt} = \frac{1}{2}\rho_f C_D A(\mathbf{u}-\mathbf{v})\|\mathbf{u}-\mathbf{v}\| + \frac{V_p\chi_m}{\mu_0\mu_r}\nabla(\mathbf{B}\cdot\mathbf{B}), \quad \ldots. (9)$$

where for spherical particles, the flow cross-sectional area $A = \pi R_p^2$, and the total particle volume $V_p = \left(\frac{4}{3}\right)\pi R_p^3$, with R_p indicating the particle radius. It is assumed that among the various forms of fluid forces on the particle, the drag force is the dominant interaction governing the particle dynamics.

To resolve the magnetic forces further, we can assume that the form of the total magnetic field at the location of the particle can be given in general as $\mathbf{B} = B_0\mathbf{f}(x)$, with $\mathbf{B}_0$ being a scalar-valued magnitude of the field and $\mathbf{f}(x)$ a geometric-spreading function that captures the spatial distribution of the magnetic field in the region of interest. Inserting this representation of the magnetic field into Eq. 9, lumping the magnetic parameters as $\alpha_m = \frac{V_p\chi_m}{\mu_0\mu_r}$, and dividing throughout by the particle mass followed by some algebraic simplifications, we obtain

$$\frac{d\mathbf{v}}{dt} = \frac{3\rho_f C_D(\mathbf{u}-\mathbf{v})\|\mathbf{u}-\mathbf{v}\|}{8\rho_p R} + \frac{\alpha_m B_0^2}{\rho_p}\nabla(\mathbf{f}\cdot\mathbf{f}). \quad \ldots\ldots (10)$$

Now the usual definition of particle-slip-velocity-based Reynolds number Re_p, and the particle-momentum-response time τ_p, can be invoked as

$$Re_p = \frac{\rho_f\|\mathbf{u}-\mathbf{v}\|(2R)}{\mu_f}, \quad \tau_p = \frac{2\rho_p R^2}{9\mu_f}. \quad \ldots\ldots\ldots\ldots (11)$$

By use of these definitions and after performing some algebraic simplifications, the motion equation for the particle can be rewritten as

$$\frac{d\mathbf{v}}{dt} = \frac{C_D Re_p}{24\tau_p}(\mathbf{u}-\mathbf{v}) + \frac{\alpha_m B_0^2}{\rho_p}\nabla(\mathbf{f}\cdot\mathbf{f}). \quad \ldots\ldots\ldots\ldots (12)$$

We can now introduce corresponding nondimensional variables for the governing variables as $\mathbf{v} = U\mathbf{v}^*$, $t = Tt^*$, and $x = UTx^*$, where the superscript * indicates a nondimensional variable. Inserting these terms into the equation of motion (Eq. 12), we obtain the following nondimensionalized form of the equation:

$$\frac{d\mathbf{v}^*}{dt} = \frac{C_D Re_p}{24St_p}(\mathbf{u}^*-\mathbf{v}^*) + \frac{\alpha_m B_0^2}{\rho_p U^2}\nabla^*(\mathbf{f}\cdot\mathbf{f}), \quad \ldots\ldots\ldots (13)$$

where the definition of the particle Stokes number $St_p = \tau_p/T$ has also been used to obtain the final result. The dynamics of the particle within the fluid domain can therefore be represented in terms of two nondimensional parameters.

The first nondimensional parameter, $\beta_{fl} \underline{\underline{\text{def}}} \frac{C_D Re_p}{24St_p} \rightarrow$, will be referred to as the drag number and denotes the competition between the particle's tendency to follow the flow-velocity field (perfect advection), and its own inertia.

The second nondimensional parameter, $\beta_{\text{mag}} \underline{\underline{\text{def}}} \frac{\alpha_m \mathbf{B}_0^2}{\rho_p U^2} \rightarrow$, will be referred to as the magnetic number and denotes the competition between the attractive forces caused by the magnetic field, and the particle inertia.

Charged Particle in an Electromagnetic Field. The motion of a charged particle in a generalized fluid volume is considered now under the action of an externally applied electromagnetic field. Proceeding similarly as before, by use of corresponding expressions for the interaction forces, we obtain the following equation of motion (where all symbols are as defined before):

$$m_p\frac{d\mathbf{v}}{dt} = \frac{1}{2}\rho_f C_D A(\mathbf{u}-\mathbf{v})\|\mathbf{u}-\mathbf{v}\| + q\mathbf{E} + q\mathbf{v}\times\mathbf{B}. \quad \ldots\ldots (14)$$

Let us assume again that the electric and magnetic fields can be represented in terms of a nondimensional spatial-spreading function as in the previous section; that is, $\mathbf{E} = E_0\mathbf{f}_e(x)$ and $\mathbf{B} = \mathbf{B}_0\mathbf{f}_b(x)$. The spatial-spreading functions $\mathbf{f}_e$ and $\mathbf{f}_b$ are similar in nature to the one defined in the previous section. Inserting these into Eq. 14, and dividing throughout by the particle mass, followed by some algebraic simplification, the following equation is obtained:

$$\frac{d\mathbf{v}}{dt} = \frac{C_D Re_p}{24\tau_p}(\mathbf{u}-\mathbf{v}) + \frac{qE_0}{m_p}\mathbf{f}_e(x) + \frac{qB_0}{m_p}[\mathbf{v}\times\mathbf{f}_b(x)]. \quad \ldots (15)$$

Introducing now the corresponding nondimensional set of variables $\mathbf{v} = U\mathbf{v}^*$, $t = \left(\frac{L}{U}\right)t^*$, and $x = Lx^*$ and inserting them into Eq. 15, followed by some algebraic simplification, the following nondimensional form of the motion equation can be obtained:

$$\frac{d\mathbf{v}}{dt} = \frac{C_D Re_p}{24St_p}(\mathbf{u}^*-\mathbf{v}^*) + \frac{LqE_0}{U^2 m_p}\mathbf{f}_e(x) + \frac{LqB_0}{Um_p}[\mathbf{v}^*\times\mathbf{f}_b(x)]. \quad \ldots\ldots\ldots\ldots (16)$$

This provides us with three dimensionless parameters to characterize the dynamics of the particle within the fluid. The first parameter is β_{fl}, the drag number defined in the previous subsection. There are two other dimensionless parameters.

System Parameters	Typical Values
Oil density	790–850 kg/m^3
Oil viscosity	0.0164–0.20 kg/m·s
Pipe radius	0.127–0.15 m
Relative magnetic permeability	5,000
Magnetic susceptibility	4,999
Assumed particle density	7870 kg/m^3

Table 1—Typical values of the governing physical parameters used for the numerical examples when using the nondimensional design parameters to explore the design-parameter space for feasible regions.

The second dimensionless parameter, $\beta_{ee} \underline{\underline{\text{def}}} \frac{q}{m_p}\frac{LE_0}{U^2} \rightarrow$, will be referred to as the electric-field number and denotes the competition between the forces caused by the applied electric field, and the particle inertia.

The third dimensionless parameter, $\beta_{em} \underline{\underline{\text{def}}} \frac{q}{m_p}\frac{LB_0}{U} \rightarrow$, will be referred to as the magnetic-field number and denotes the competition between the forces cause by the applied magnetic field, and the particle inertia.

Implications for Design: Numerical Examples. The starting point in designing a strategy for healing a specific location in the pipe would be the quick identification of feasible parameters that lead to efficient migration of particles to the desired location. The nondimensional parameters obtained by use of the analyses presented thus far can aid efficient exploration of the parameter space, and identify feasible regions. To illustrate this, two examples are presented here. **Table 1** presents the characteristic values for various physical parameters used in the examples, which are realistic values obtained from a survey of existing literature and data.

Considering the case that used uncharged-iron-filing particles released inside a pipe and guided by use of an externally applied magnetic field, the particle size R, the magnetic field strength $\mathbf{B}_0$, and the characteristic flow velocity U can be used to define the parameter space. **Fig. 2a** compiles the curves along which $\beta_{\text{mag}} = \beta_{fl}$, for varying pipe-flow velocities. This chart can now be used to identify feasible combinations for design. Specifically, any combination of $(B_0,\ U,\ R)$ for a chosen U that lies above the corresponding curve on the parameter space in Fig. 2a will lead to magnetic interactions being dominant. In addition, Fig. 2b represents the variation in the magnitude of $\beta_{\text{mag}}/\beta_{fl}$, for a characteristic flow velocity of 1 m/s, for varying particle sizes and field strengths. Physically, a feasible design would entail a higher value of this ratio, thereby indicating that the magnetic interactions dominate the dynamics of the particle motion as opposed to the fluid/particle interaction. Similar to the chart in Fig. 2a, regions in this space of B_0 and R indicated in blue will therefore be "bad" regions, whereas regions in red will be "good" regions from a design perspective. Particle sizes are measured in meters, whereas magnetic-field strength is measured in Tesla.

Similar calculations can also be performed for guiding charged particles to a location by use of electric or magnetic fields. It is remarked here that although the charge on the particle appears as a parameter in β_{ee} and β_{em}, there are in reality limits to the amount of charge that an individual particle can carry. This primarily results from a balance between the repulsion among the elementary charges carried on the particle and the particle's surface potential (Liu and Pui 1974). This limiting charge is a function of the particle size and also of the charging mechanism. It can be shown that the limiting charge can be reasonably approximated by use of

$$\log(q) = C_1 \log(2R) + C_2,$$

where C_1, C_2 are coefficients that are dependent on the charging mechanism. By use of the correlations presented by Liu and Pui (1974), the values of these coefficients were approximated, and used thereafter as inputs to the analysis. With this consideration, for charged particles flowing in a pipe and guided by an electric field, the curves for $\beta_{ee} = \beta_{fl}$ have been presented in **Fig. 3a.** Similar to the previous example, a combination of parameters (E_0, R) that fall below this line for a chosen flow velocity U will be an infeasible choice for the application desired, because fluid forces will dominate particle behavior. Similarly, to illustrate the applicability to a magnetic field—referred to as B-field in Fig. 3b—for guiding a charged-particle stream, the contours of the ratio β_{em}/β_{fl} have been compiled for a characteristic-flow velocity of 1 m/s in Fig. 3b. Again, feasible regions correspond to a higher value of this ratio (that is, magnetic forces dominate particle behavior), which has been identified in red, whereas infeasible or "bad" regions are indicated in blue. It is noted here that in all these examples, a relatively wide range of velocities has been chosen to better identify the upper and lower bounds for the model predictions.

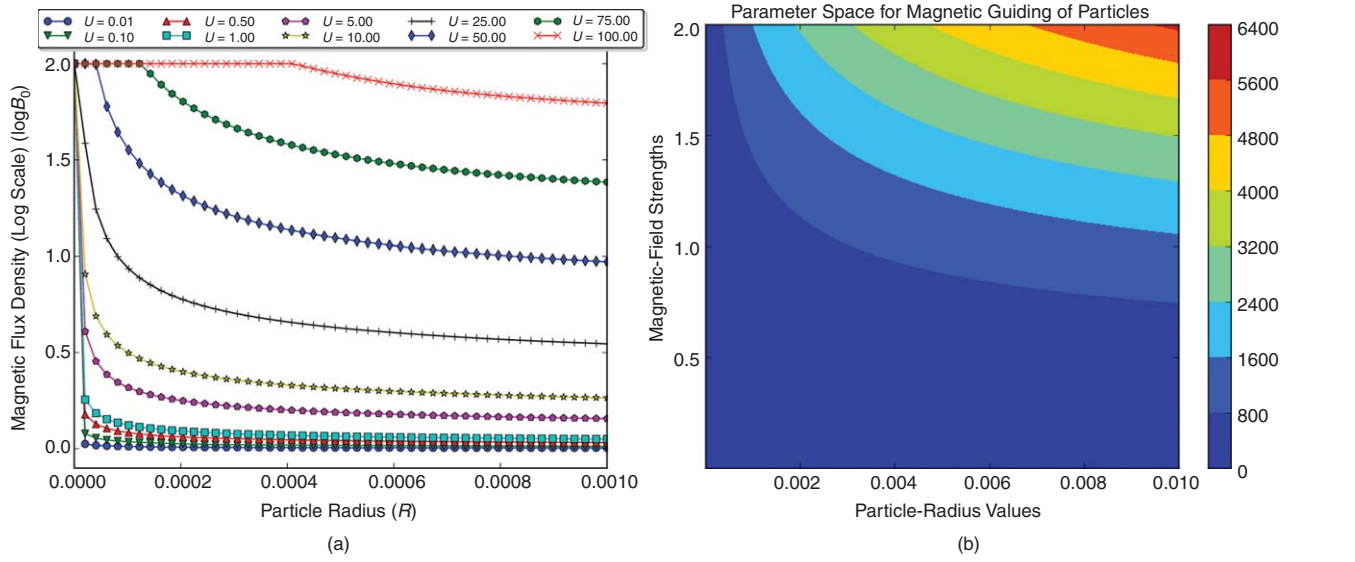

Fig. 2—(a) Curves for parameter combinations (B_0, U, R) that lead to $\beta_{\text{mag}}=\beta_{fl}$ are presented. (b) Contour plot illustrating the variation in values of $\beta_{\text{mag}}=\beta_{fl}$ for varying combinations of field strengths and particle sizes for a flow velocity of 1 m/s. Velocity is in m/s, particle radii are in meters, and magnetic field strength is in Tesla. Note that these particles are uncharged.

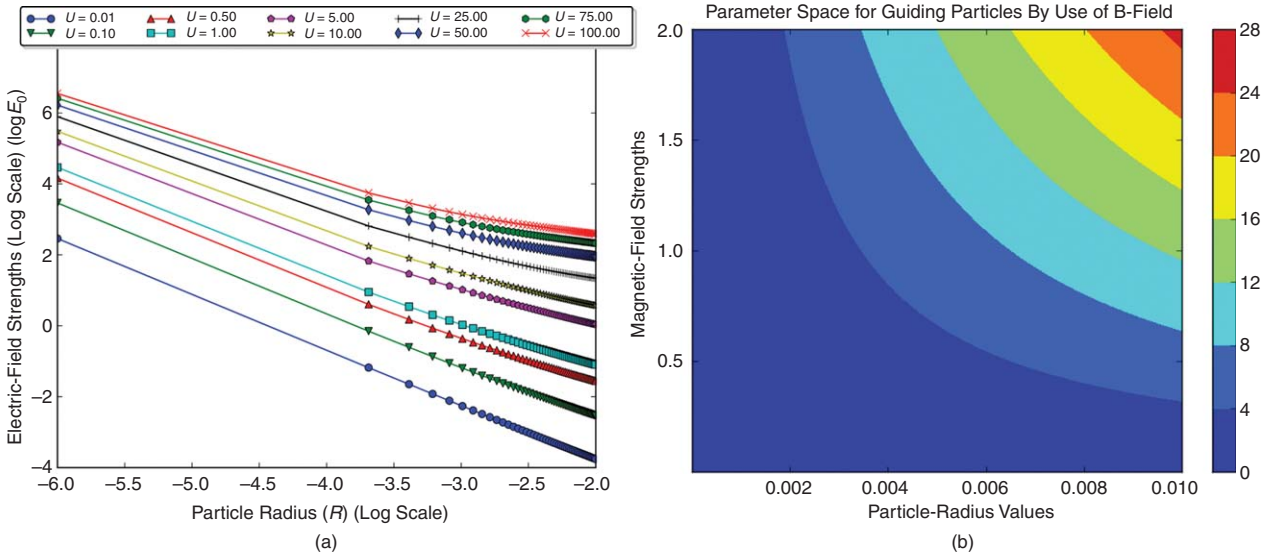

Fig. 3—(a) Curves along which $\beta_{ee}=\beta_{fl}$ for varying flow velocities are presented. (b) Contours of the ratio β_{em}/β_{fl} for a specified flow velocity of 1 m/s. The charge limit is assumed to be the maximum, modeled as $\log(q)= C_1\log(2R) + C_2$ to consider the best-case scenario for electromagnetic control. Velocity is in m/s, particle radii are in meters, and electric-field strength is in Newtons/Coulomb (N/C).

3D Discrete-Element-Method Modeling and Simulation Framework

Flow-Velocity Profile. For a one-way-coupled fluid/particle-interaction model, information on the velocity field for the fluid is a necessary boundary condition. With the coupling being one-way, particles do not affect the flow field significantly. Hence, fluid-velocity fields, obtained analytically by use of existing solutions of the Navier-Stokes equations for representative simple-flow problems, or numerically by use of computational-fluid-dynamics techniques, can be used directly as input for the simulation of collective particle dynamics. For the current work we adopt the former, and it is assumed that the steady, fully developed, longitudinal-flow velocity within the pipe can be represented as

$$\mathbf{u} = U \cdot s\left(\frac{r}{R_{\text{pipe}}}\right)\hat{\mathbf{x}}, \quad \ldots\ldots\ldots\ldots\ldots\ldots\ldots\ldots\ldots (17)$$

where $s(\cdot)$ denotes a geometric-spreading function that governs the variation of flow velocity across radial locations and U is the characteristic-flow velocity, as before. A good choice for this spreading function can be presented as

$$s\left(\frac{r}{R_{\text{pipe}}}\right) = \left(\gamma + \frac{2}{\gamma}\right)\left[1 - \left(\frac{r}{R_{\text{pipe}}}\right)^{\gamma}\right], \quad \ldots\ldots\ldots\ldots (18)$$

with γ being a parameter that governs the shape of the flow profile for various flow regimes. In precise terms, when $\gamma = 2$, then the flow profile is quadratic, which is the typical profile for fully developed, laminar Newtonian flow within a pipe obtained by a direct solution of the Navier-Stokes equations for steady pipe flow. For turbulent flows, or for other flow variations, this profile may become flatter or rounder, which can be modeled by use of an appropriately chosen value of γ.

Particle/Particle-Contact Interactions. Particle migration toward the target location will be dependent upon the collisional interactions between flowing particles, which has been modeled in the simulation framework by use of linear- and angular-momentum balances along directions normal and tangential to the line joining particle centers **(Fig. 4a).** The normal- and tangential-direction vectors can be calculated for a pair of colliding particles (indexed by i and j) by

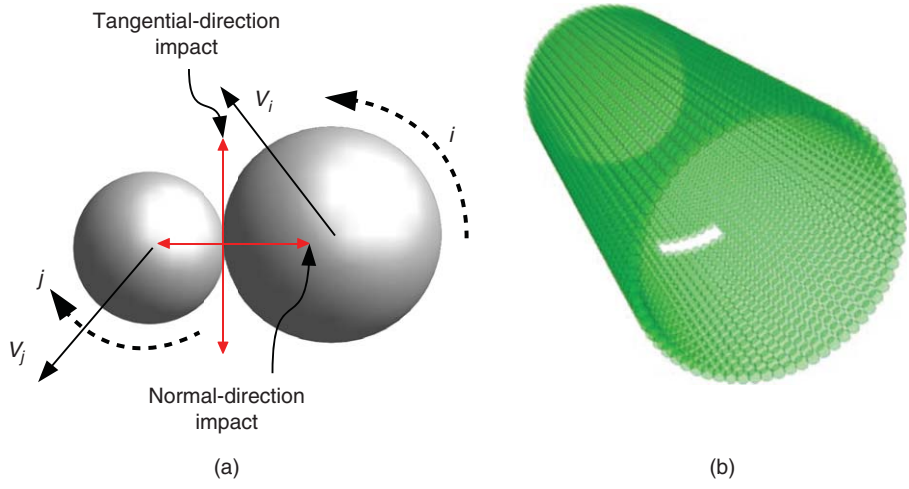

Fig. 4—(a) Typical schematic for modeling impulse-momentum-based contact-force modeling. (b) Computational representation of the curved pipe wall with a damaged location, recreated by use of combinations of spherical particles.

$$\hat{\mathbf{n}}_{ij} = \frac{x_i - x_j}{\|x_i - x_j\|}\,,\ \hat{\mathbf{t}}_{ij} = \frac{\mathbf{v}_{\rm rel} - (\mathbf{v}_{\rm rel}\cdot\hat{\mathbf{n}}_{ij})\hat{\mathbf{n}}_{ij}}{\|\mathbf{v}_{\rm rel} - (\mathbf{v}_{\rm rel}\cdot\hat{\mathbf{n}}_{ij})\hat{\mathbf{n}}_{ij}\|}, \quad \ldots\ldots\ldots (19)$$

where $\mathbf{v}_{\rm rel}$ is the relative velocity between the spheres at the point of contact, and is given by $\mathbf{v}_{\rm rel} = (\mathbf{v}_j - \mathbf{v}_i) + (\omega_j \times R_j\hat{\mathbf{n}}_{ij} - \omega_i \times R_i\hat{\mathbf{n}}_{ij})$. Balancing pairwise linear momenta for the collision duration δt is as follows:

$$m_i\mathbf{v}_i(t+\delta t) - m_i\mathbf{v}_i(t) = \langle\mathbf{F}_i^c\rangle\delta t + \langle\mathbf{F}_i^e\rangle\delta t, \quad \ldots\ldots\ldots (20)$$

$$m_j\mathbf{v}_j(t+\delta t) - m_j\mathbf{v}_j(t) = \langle\mathbf{F}_j^c\rangle\delta t + \langle\mathbf{F}_j^e\rangle\delta t, \quad \ldots\ldots\ldots (21)$$

where the superscripts c and e denote the contact forces and external, noncontact forces, respectively, and δt denotes the compression duration. The inelastic effects, owing to the work performed by mechanical forces within the bulk of the contacting particles to cause inelastic deformations, are incorporated in the system dynamics by use of the restitution coefficient (e). Decomposing the overall contact event into a compression phase (where the particles approach each other as they decelerate), and a recovery phase (where the particles recede from each other), the restitution coefficient can be defined as the ratio between the contact impulse during recovery phase to that during compression phase. For perfectly elastic collisions, we have $e = 1$, and for perfectly inelastic collisions, we have $e = 0$. Assuming further that the total contact force for the pairwise collision on particle i can be written in terms of a normal contact component (f_N) and a tangential contact component (f_T) as $\mathbf{F}_i^c = f_N\hat{\mathbf{n}}_{ij} + f_T\hat{\mathbf{t}}_{ij}$, and performing appropriate algebraic simplifications, the following expression for the total normal contact force can be obtained:

$$\langle f_N\rangle\delta t = \frac{1+e}{m_i+m_j}(m_i\langle F_{jn}^e\rangle_c\delta t_1 - m_j\langle F_{in}^e\rangle_c\delta t_1) - \frac{(1+e)m_im_j}{m_i+m_j}[\mathbf{v}_{in}(t) - \mathbf{v}_{jn}(t)], \quad \ldots\ldots\ldots (22)$$

where subscript n indicates components of the corresponding vectors along $\hat{\mathbf{n}}_{ij}$, the operation $\langle\cdot\rangle_c$ denotes average over the compression phase of the collision, and δt_1 is the compression duration of the collision.

It is assumed that the colliding and flowing particulate stream will not involve particles engaging in enduring contacts with each other. For such cases, the exact stick/slip treatment of Coulomb friction can be relaxed, and for the tangential component of the contact impulse a regularized form of the Coulomb friction model can be used. Such regularized models can lead to robust numerical methods for integrating the motion equations. Further discussions on regularized Coulomb friction models can be found in Oden and Pires (1984) and Wriggers and Zavarise (2002). In general, the friction force can be given by

$$\langle f_T\rangle = \mu\mathcal{R}(v_{{\rm slip},t})\|f_N\|, \quad \ldots\ldots\ldots (23)$$

where $\mathcal{R}(v_{{\rm slip},t})$ is a regularization function that approximates the discontinuity of classical stick/slip Coulomb friction law, and is a function of the tangential-relative-slip velocity. For the present work, a commonly used piecewise continuous form of $\mathcal{R}(v_{{\rm slip},t})$ has been chosen, as follows:

$$R(v_{{\rm slip},t}) = \begin{cases} -1, & \forall\ v_{{\rm slip},t} < -\epsilon \\ \dfrac{v_{{\rm slip},t}}{2\epsilon}, & \forall\ -\epsilon < v_{{\rm slip},t} < \epsilon \\ 1, & \forall v_{{\rm slip},t} > \epsilon \end{cases}, \quad \ldots\ldots\ldots (24)$$

where ϵ is a regularization parameter, and smaller values of this parameter lead to better approximation of the stick/slip law.

To balance the angular momenta, we define a third unit vector $\hat{\mathbf{s}}_{ij} = \hat{\mathbf{n}}_{ij} \times \hat{\mathbf{t}}_{ij}$, to complete a triad. The total angular-momentum balance can now written in terms of the components along $\hat{\mathbf{s}}_{ij}$ by use of the torque caused by the tangential-contact impulses, as follows:

$$I_i\omega_{is}(t+\delta t) = I_i\omega_{is}(t) + R\mu\mathcal{R}(v_{{\rm slip},t})\|f_N\|\delta t + \langle M_{is}^e\rangle\delta t, \quad \ldots\ldots\ldots (25)$$

$$I_j\omega_{js}(t+\delta t) = I_j\omega_{js}(t) - R\mu\mathcal{R}(v_{{\rm slip},t})\|f_N\|\delta t + \langle M_{js}^e\rangle\delta t, \quad \ldots\ldots\ldots (26)$$

where M_{is}^e and M_{js}^e are the corresponding components of all external moments acting on the respective particles during the collision.

Particle Interactions With Pipe Wall. To accurately model the interaction of the flowing particles with the curved walls of the cylindrical pipe, the pipe wall was reconstructed by use of a collection of spherical particles as computational units. These wall particles are treated to be stationary throughout the simulation, and their interaction with a corresponding flowing particle is resolved by use of the contact-force models presented in the previous section. Such methods often find use in dynamic simulations of particle systems for considering wall boundaries, as discussed by Pöschel and Schwager (2005), among others. A significant computational advantage that such a representation of the pipe wall provides is in terms of the flexibility to model a damaged location on the pipe wall. This can be performed either by completely removing the particles from that location or by replacing them with particles of smaller radii. An illustration of this has been presented in Fig. 4b, where wall particles are indicated in green, and a damaged site is created in the middle of the pipe by removing a patch of particles.

Solution Algorithm for System Dynamics. The overall dynamics of the system of particles for combined electromagnetic interactions, fluid/particle interactions, and particle/particle- and particle/wall-contact interactions can be represented by use of the following form of the motion equation for any particle i in a system of N_p particles (the term $\mathbf{F}_{i,\rm mag}$ will be used as a placeholder for both magnetic forces and Lorentz forces on charged particles):

$$m_i\frac{{\rm d}\mathbf{v}_i}{{\rm d}t} = \sum_{i=1}^{N_s}\mathfrak{T}(i,\mathcal{S}_j)\mathbf{F}_{ijs,\rm contact} + \sum_{j\neq i,j=1}^{N_p}\mathfrak{T}(i,j)\mathbf{F}_{ij,\rm contact} + \mathbf{F}_{i,\rm fluid} + \mathbf{F}_{i,\rm mag}, \quad \forall i = 1,2,\ldots,N_p, \quad \ldots\ldots\ldots (27)$$

$$\frac{{\rm d}\mathbf{x}_i}{{\rm d}t} = \mathbf{v}_i, \forall i = 1,2,\ldots,N_p, \quad \ldots\ldots\ldots (28)$$

where computational particles used to represent the pipeline wall have been referred to as $\mathcal{S}_j$ and the term $\mathfrak{T}(\cdot,\cdot)$ is an indicator function indicating contact between a pair of particles. This indicator function is evaluated as follows for spherical particles:

$$\mathfrak{T}(i,j) = 1, \quad \text{if } \|\mathbf{x}_i - \mathbf{x}_j\| \le R_i + R_j \Rightarrow \text{contact occurs}, \quad \ldots\ldots\ldots (29)$$

$$\mathfrak{T}(i,j) = 0, \quad \text{if } \|\mathbf{x}_i - \mathbf{x}_j\| > R_i + R_j \Rightarrow \text{no contact}. \quad \ldots\ldots\ldots (30)$$

To speed up pairwise checks for evaluating contact forces, typical binning and domain-partitioning techniques have been implemented. Such techniques have been discussed in detail in Chialvo and Debenedetti (1990) and Pöschel and Schwager (2005), for example and ensure that potential contact searches are performed only between nearest neighbors, whereas particles far away are rejected from the search. The individual particles may also be considered to be undergoing variations in rotational motion and temperature. However, keeping with the scope of the present work to outline the development of the algorithm, these have not been considered here. The motion equations have thereafter been solved by use of a generalized one-step ϕ-type timestepping scheme,

1: Generate particle mesh for cylinder wall
2: Set up fluid-velocity profile
3: Set $\Delta t \leftarrow$ timestep size; set $T_{\text{sim}} \leftarrow$ simulation time
4: For $\left[t \le mod\left(\frac{T_{\text{sim}}}{\Delta t}\right) \right]$, do
5: Inject particles
6: While (iteration error ≤ tolerance)
7: $\mathbf{F}_{ij}^{c} \leftarrow$ build all contact forces: $\forall i, j = 1,\cdots, N_p$
8: $\mathbf{F}_{ij}^{fl} \leftarrow$ build all fluid forces: $\forall i = 1,\cdots, N_p$
9: $\mathbf{F}_{ij}^{\text{mag}} \leftarrow$ build all magnetic forces: $\forall i = 1,\cdots, N_p$
10: Resolve which particles have arrived at target location
11: If (particle i is not at target location), then
12: Particle rebounds with $\mathbf{F}_{i}^{c} \leftarrow$ contact force between particle and surface
13: End if
14: Calculate total force $\leftarrow \mathbf{F}_{ij}^{c} + \mathbf{F}_{i}^{c} + \mathbf{F}_{i}^{fl} + \mathbf{F}_{i}^{\text{mag}}$
15: For (particle $id = 1, N_p$), do
16: Update particle velocity (by use of Eqs. 27 and 31)
17: Update particle position (by use of Eqs. 28 and 32)
18: End for
19: Calculate iteration error (by use of Eq. 34)
20: End while
21: Conditionally dump particle data to external file for post-processing
22: End for

Table 2—Pseudocode for the implementation of the numerical framework, outlined here into a computer code.

$$\mathbf{v}_i^{N+1} - \mathbf{v}_i^{N} = \frac{\Delta t}{m_i}\left[\phi \mathbf{F}_i^{N+1} + (1-\phi)\mathbf{F}_i^{N}\right], \quad \ldots\ldots\ldots\ldots (31)$$

$$\mathbf{x}_i^{N+1} - \mathbf{x}_i^{N} = \Delta t\left[\phi \mathbf{v}_i^{N+1} + (1-\phi)\mathbf{v}_i^{N}\right], \quad \ldots\ldots\ldots\ldots (32)$$

where the superscript N indicates the timestep index. Such schemes have been found to be very flexible for simulations of particle systems, as illustrated in Zohdi (2007, 2010). In general, the forces are dependent on particle-ensemble positions and velocities, thereby requiring an iterative solution of Eqs. 31 and 32. The iterations are performed by use of a fixed-point-contraction scheme, which in its general form can be illustrated by use of the velocity updates as

$$\mathbf{v}_i^{N+1,K+1} = \frac{\Delta t \phi}{m_i}\mathbf{F}_i^{N+1,K} + \left[\frac{\Delta t}{m_i}(1-\phi)\mathbf{F}_i^{N} + \mathbf{v}_i^{N}\right], \quad \ldots\ldots (33)$$

with the superscript K indicating the iteration index. The termination criteria for the iterative solutions at each timestep are governed by the overall phase-space-iterative error, defined as

$$e_{\text{iter}} = \sum_i \frac{\|\mathbf{v}_i^{N+1,K+1} - \mathbf{v}_i^{N+1,K}\| + \|\mathbf{x}_i^{N+1,K+1} - \mathbf{x}_i^{N+1,K}\|}{\|\mathbf{v}_i^{N+1,K+1} - \mathbf{v}_i^{N+1,0}\| + \|\mathbf{x}_i^{N+1,K+1} - \mathbf{x}_i^{N+1,0}\|}, \quad \ldots\ldots\ldots\ldots\ldots\ldots (34)$$

where the superscript 0 indicates the initial guess for iterative solution at each timestep, and iterations are terminated once e_{iter} falls below a chosen error tolerance. At the inlet boundary, an injection-type boundary condition for the particles is devised, where particles are introduced uniformly and randomly on the inlet plane at every timestep. Particle centers that reach the outlet plane are thereafter considered to exit the simulation domain permanently. The model for the adhesion and further treatment of the particles upon migration to the target site could be a complicated multiphysical process, and a detailed model for the same would be beyond the scope of this work. To focus on the aspect of accumulation of particles at a location, a simplified approach is incorporated on the basis of recreating a damaged target zone in the pipe wall by removing a set of wall particles, and assuming that migrated particles that fill this location and do not bounce off are considered to be computationally stuck to the location. The flexibility of the overall framework, however, allows for more-complicated near-wall interaction models to be incorporated easily. The computational implementation of the framework has been outlined in the form of a pseudocode in **Table 2.**

Case Study for Benchmarking the Numerical Framework

A precise design of physical experiments, data collection, and analysis for the magnetically guided process is beyond the scope of the current work. An additional benchmark study was performed to establish the validity of the numerical-simulation framework presented here. The case study was modeled after the work on single-particle motion in a microchannel by Sinha et al. (2007). In their original work, Sinha et al. (2007) presented experimental data on magnetically guiding a single microparticle (1−μm diameter) within a microchannel of aspect ratio 1:20 by use of a spatially nonuniform magnetic field. The motion of the magnetic microbead is tracked by use of a digital zoom microscope coupled with an additional objective lens with a magnification of 1,000X. A simple model for the particle motion is also presented where the quasisteady motion of the particle is modeled by equating the magnetic force to the Stokesian drag on the particle. The particle velocity is therefore obtained as

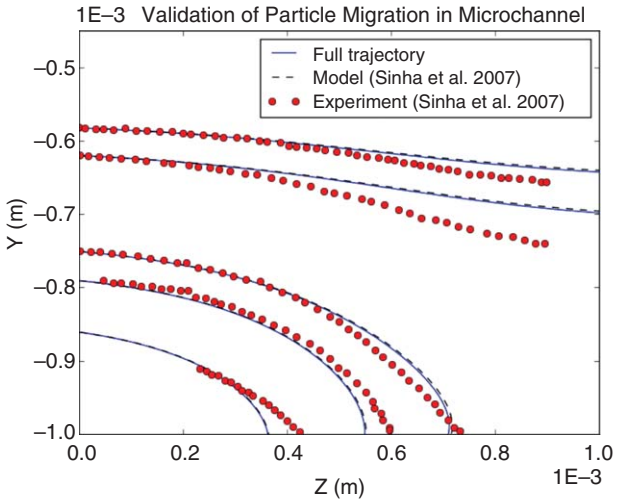

Fig. 5—Benchmark comparison of the numerical framework developed in this work with experimental study on single-particle motion in microchannels presented by Sinha et al. (2007).

$$\mathbf{v}_i(x,y) = \frac{1}{6\pi\mu_f(2R_i)}\mathbf{F}_i^{\text{mag}} + \mathbf{u}(x,y), \quad \ldots\ldots\ldots\ldots \quad (35)$$

and the particle position is then obtained by a direct numerical integration as follows:

$$\mathbf{x}_i(t) = \int_0^t \mathbf{v}_i(x,y,\tau)\mathrm{d}\tau + \mathbf{x}_i(x,y,0). \quad \ldots\ldots\ldots\ldots\ldots\ldots (36)$$

Sinha et al. (2007) provide additional details on the system parameters and experimental details in their work. For the present work, the model for the particle motion has been implemented within the numerical framework developed herein. Unlike the original work, the full motion equation of the particle incorporating the particle acceleration, buoyancy, and gravity has been solved by use of the framework outlined in Table 2. Particle/wall collisions and multiple-particle collisions were not incorporated in the original work, and hence have been suppressed in this comparative study. The Stokes-drag equation was replaced by the standard form of the drag force, as presented in Eq. 2. The form of the fluid-flow profile and the spatial distribution of the magnetic field were retained to be the same as in the original work. The framework, therefore, includes a more-complete model of the physical interactions at the particle level. A comparison of the experimental data, and the results from the simple model by Sinha et al. (2007), with the results for particle trajectory obtained by use of the current simulation framework are presented in **Fig. 5.** The results match the experimental data reasonably well, and minor variations in the trajectories obtained by the two different numerical models are observed as expected. The variations between experimental and calculated (from both models) data can be attributed to the variability in modeling the exact magnetic field caused by a magnet by use of an analytical function, as presented by Sinha et al. (2007).

Numerical Example for a Magnetically Guided Noninvasive Healing Procedure

The implementation of the developed models and framework is illustrated by use of a representative-model problem for a magnetically guided particle stream. The schematic configuration in Fig. 1a has been used to set up the model problem. A cylindrical pipe of unit length is modeled with a damaged location at the center of the pipe; the dimensions of the damage have been exaggerated in the model to aid easy visualization of the particles migrating to the target site. Magnetic (uncharged) particles of size 200 μm are released from rest at the inlet plane into a steady, fully developed flow. The magnetic field is assumed to be of the form

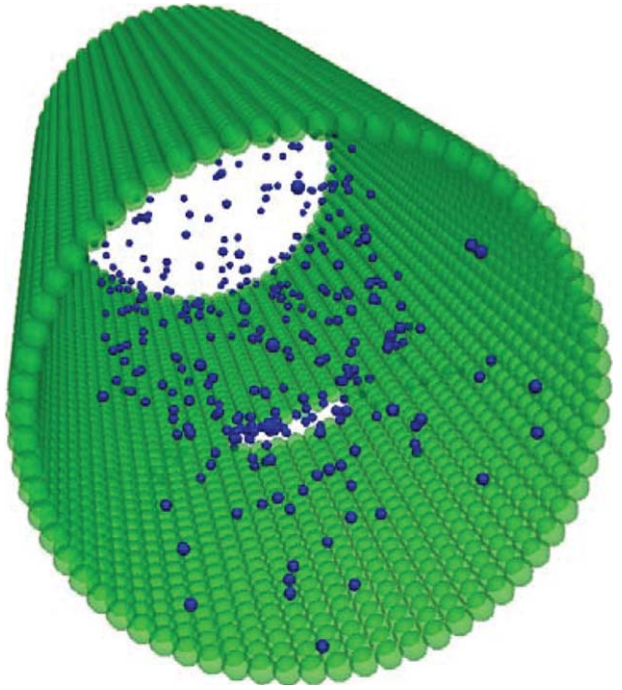

Fig. 6—Snapshot of simulation data to illustrate the typical spatial distribution of the particles in the presence of the background fluid flow and a magnetic field guiding them toward the damage location.

$$\mathbf{B} = B_0 e^{-\alpha(\mathbf{x}_i-\mathbf{x}_p)\cdot(\mathbf{x}_i-\mathbf{x}_p)} \frac{\mathbf{x}_i-\mathbf{x}_p}{\|\mathbf{x}_i-\mathbf{x}_p\|}, \quad \ldots\ldots\ldots\ldots \quad (37)$$

which satisfies the assumptions made earlier. The magnetic field is active in the region where the damage has occurred, and truncated everywhere else. Velocities and positions of all particles in the pipe at each instant are updated by use of the algorithm summarized in Table 2. To visualize the fully 3D scatter of particles during the transport process, a typical, representative snapshot of particle positions is shown in **Fig. 6,** where oncoming particles, particles rebounding from the walls, particles colliding with each other, and particles reaching the target region lead to a scattered arrangement of particles distributed in the carrier fluid.

An illustration of how the particle system evolves with time as the particles are guided toward the target location by the magnetic field, and then are allowed to fill up the void created in the pipe wall, is presented in **Figs. 7a through 7h,** sequentially from top-left to bottom-right, for a total simulation time of 1 second. All temporal snapshots are viewed laterally, along a longitudinal sectional view of the pipe segment. The pipe-wall particles have been rendered translucent, thereby aiding visualization of particle motion. A fraction of the incoming particle stream constantly keeps migrating to, and accumulating at, the target site. The collisions with the pipe walls cause many of the particles to drift into the stream of oncoming particles and get scattered because of further interparticle collisions, which leads to variability in the number of particles arriving at the location of the damage. Therefore, it is evident that while increasing the particle-number density may cause an increase in the number of particles accumulating at the target site, it may also increase chances of interparticle collisions and scattering if insufficient magnetic-field strengths are used. After the discussion regarding parameter selection, the magnetic-field strength $\mathbf{B}_0$ was chosen to correspond with the chart presented in Fig. 2a. Specifically, for the particle size and for pipe-flow velocity in the range of 1–10 m/s, by use of Fig. 2a we choose a field-strength ($\mathbf{B}_0$) value of 1.5 T, which is sufficiently above the curve corresponding to $\beta_{\text{mag}} = \beta_{fl}$ for all velocities in that range. The rest of the particle and fluid properties are chosen by use of Table 1. We remark that while the particle radius used is 200 μm, particles are enlarged in the pictures so that they can be visualized in the snapshots.

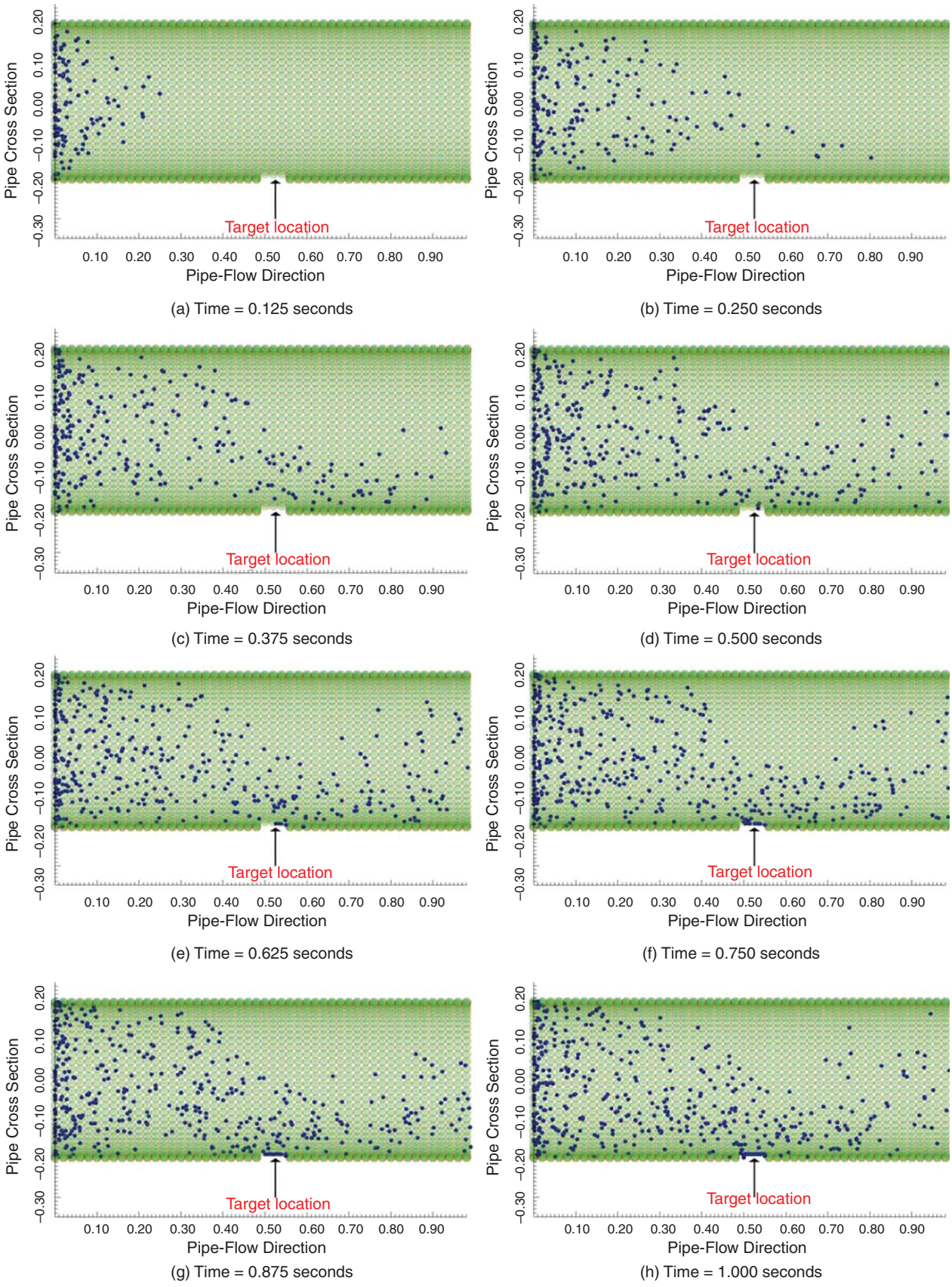

Fig. 7—(a)–(h) Snapshots in time illustrating the dynamics of the magnetically guided particle stream, and particle accumulation at the damage site, for an imposed centerline flow velocity of 5 m/s. Pipe length of 1 m, with pipe radius scaled to 0.2 times the pipe length.

As a further illustration of the competition between the magnetic interactions, the fluid/particle interactions, and the interparticle-contact interactions, the simulations were repeated with different flow velocities while all other parameters were held constant. Increased flow velocities will lead to a reduced value of the magnetic number β_{mag} and lead to slower accumulation of particles at the target location. This is also the trend observed from the simulations, and a simple illustration of this trend is presented

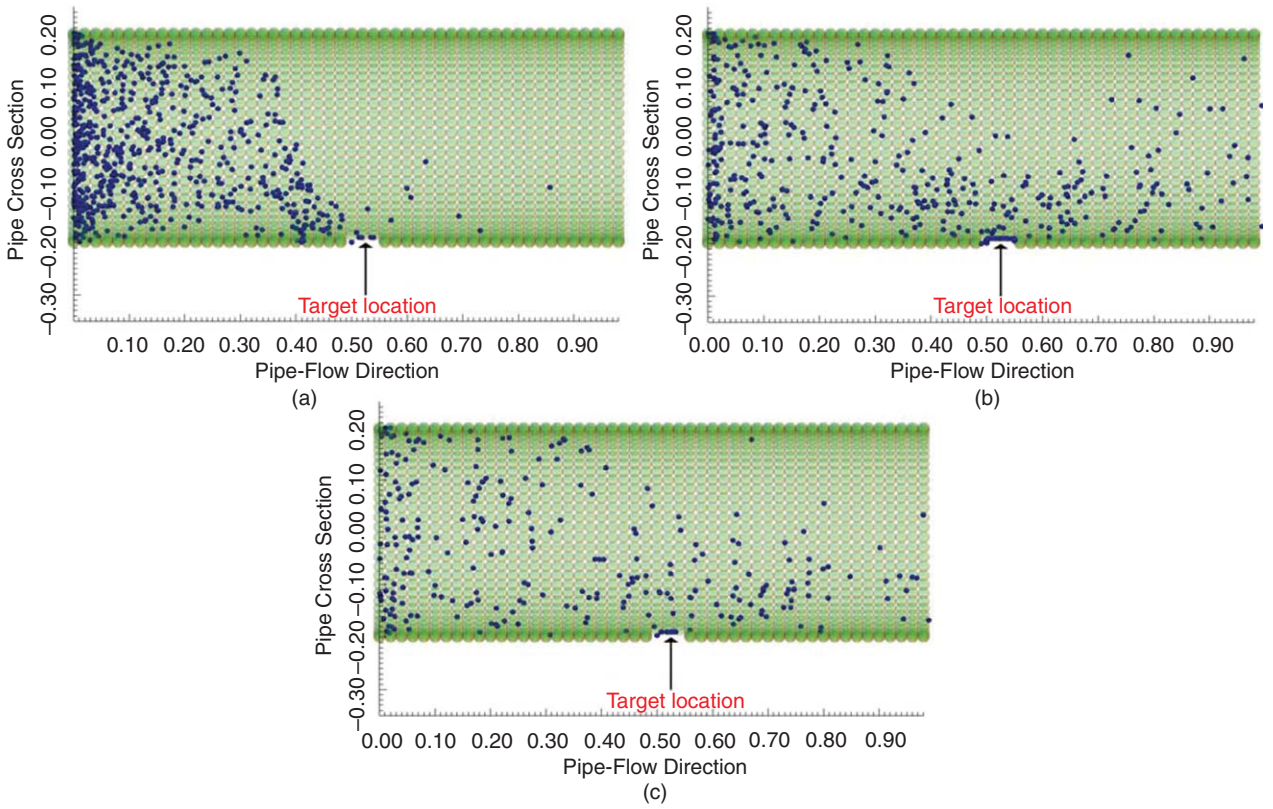

Fig. 8—Particles accumulating toward a target site for imposed pipe-flow velocities of (a) 1 m/s (left), (b) 5 m/s (right), and (c) 10 m/s (bottom) after 1 second of simulation time. Pipe length of 1 m with pipe radius scaled to 0.2 times the pipe length.

in **Fig. 8,** in which final particle accumulation after 1 second of simulation time for flow velocities of 1, 5, and 10 m/s has been presented. As the flow velocity reduces, larger numbers of particles are deviated by the magnetic field, and lesser particles escape the pipe segment being simulated. It is also noted here that while much of the scattering of particles for the higher flow velocities is observed distal to the target site, most of the collisional scattering of particles for the lower flow velocities actually occurs before the target site, thereby affecting the efficiency of particle migration to the target site. Similar trends were also observed for reduced magnetic-field strengths and for rapid spatial variations of the magnetic-field strength (which is quantified in the simulations by use of the geometry parameter α for the magnetic field). This evidence points to the critical role played by particle-number density or concentration in governing process efficiency, which is an aspect currently being investigated further by the authors.

Concluding Remarks

This work presents the theoretical models and a computer-simulation framework for design and analysis of a noninvasive pipe-healing technique by use of electromagnetically guided particles released into the pipe interior. The basic physical principles that govern such a process have been outlined, along with models for the use of the physical principles to create an appropriate design space for such techniques. This has been illustrated by use of simple numerical examples. The primary modeling assumptions include a one-way-coupled fluid/particle interaction, neglecting interparticle magnetic interactions, assuming a linear magnetic material, assuming a physically realistic steady-flow profile, and assuming collisionally interacting particles such that exact stick/slip friction is replaced by a modified-sliding-friction model for contact. Physical models of particle-level interactions have been thereafter used to construct a discrete-element-method framework for detailed simulations of such a technique. The framework is implemented here assuming the flow is single-phase; however, because one-way coupling assumes that known flow velocities are inputs to the particle system, the framework can be easily extended to multiphase flows. The critical aspects of the simulation algorithm have been discussed in detail along with a complete pseudocode to assist practicing researchers in implementing the framework, and the implementation of the framework has been illustrated by use of a model problem of magnetically guided particle streams for interior-damage repair of piping walls. The analysis of the design space by use of similitude parameters outlined the fundamental aspect of competition between the fluid/particle interaction, and the interaction caused by applied electromagnetic fields. The discrete-particle-simulation framework considers further details of process physics, including variations in flow profile, spatial variations in the applied electromagnetic fields, influence of particle/particle and particle/wall collisions, and time scale of response of the particles to the background flow. Although a simple analytical form for the magnetic field is used here, the exact form of the field is not key to the development of the framework. Any other form of the magnetic-field description—obtained from other data or experiments—can be easily used as an input to the framework, thereby making it general enough. The overall simulation framework is validated by use of a benchmark study on trajectory of a single particle in a microchannel, and the model captures the physical characteristics of the particle motion very well. It is noted here that additional aspects, such as influence of wall thickness on applied electromagnetic fields, influence of two-way-coupling phenomena on the nature of fluid/particle interactions, and detailed calculations of particle-accumulation times and process-efficiency metrics, have not yet been incorporated here. In addition, a detailed model for a safe, noninvasive fusion treatment of the accumulated particles to complete the repair process has also not been incorporated in this work, and for this purpose, obtained properties of the repaired area and its impact on pipeline integrity are important considerations. Also, the effect of corrosion on the pipe wall because of the carrier fluid and the efficiency of corrosion inhibitors in the presence of particles have not been considered in this work. These are issues that are being currently investigated by the authors as further advancements to the theory and model presented herein. Owing to the flexibility of the discrete-element technique,

however, such additional details can be incorporated into the framework developed here relatively easily.

Nomenclature

Please note that H denotes Henry, the unit for magnetic inductance; T denotes Tesla, the unit of magnetic field strength; A denotes ampere, the unit for electric current strength; N denotes Newton, the unit for force; and C denotes Coulomb, the unit for charge.

A = cross-sectional area of the particle, m^2
$\mathbf{B}$ = magnetic field vector
B_0 = magnetic field strength, T
C_D = drag coefficient, nondimensional
e = restitution coefficient for contact, nondimensional
$\mathbf{E}$ = electric field vector
E_0 = electric field strength, N/C
$\mathbf{f}_b$ = nondimensional geometric spreading function for $\mathbf{B}$
$\mathbf{f}_e$ = nondimensional geometric spreading function for $\mathbf{E}$
$\mathbf{H}$ = magnetic-field-intensity vector, A/m
I_p = particle moment of inertia, kg/m
L = characteristic mean length scale, m
m_p = mass of the particle (indicated by subscript p), kg
$\mathbf{M}$ = magnetization vector, A/m
$\hat{n}_{ij}, \hat{t}_{ij}, \hat{s}_{ij}$ = orthogonal triad for resolving contact forces between particles
q = particle charge, C
r = pipe radial coordinate, m
R_p = radius of the particle (indicated by subscript p), m
Re_p = Reynolds number based on the particle-slip velocity, nondimensional
St_p = particle Stokes number, nondimensional
T = characteristic mean time scale, seconds
$\mathbf{u}$ = carrier-fluid velocity vector, m/s
U = characteristic mean velocity, m/s
$\mathbf{v}$ = particle velocity vector, m/s
$\mathcal{V}$ = volume (with the appropriate subscripts for particles), m^3
γ = nondimensional spreading factor
Δt = timestep for simulations, seconds
$\Delta\phi$ = nondimensional discretization parameter
μ = restitution friction coefficient for contact, nondimensional
μ_0 = permeability of free space ($= 4\pi 10^{-;7}$ H/m)
μ_f = carrier fluid viscosity, Pa·s
μ_m = magnetic moment, N·m/T
ρ_f = carrier fluid density, kg/m^3
ρ_p = density of the particle (indicated by the subscript p), kg/m^3
τ_p = particle momentum response time, seconds
χ_m = magnetic susceptibility, nondimensional
ω = particle angular velocity, radians/s
$\mathfrak{T}(\alpha, \beta)$ = nondimensional indicator function for contact between α and β

References

Bailey, A. and Hiatt, J. 1972. Sphere Drag Coefficients for a Broad Range of Mach and Reynolds Numbers. *AIAA J.* **10** (11): 1436–1440. http://dx.doi.org/10.2514/3.50387.

Berlemont, A., Desjonqueres, P. and Gouesbet, G. 1990. Particle Lagrangian Simulation in Turbulent Flows. *Int. J. Multiphas. Flow* **16** (1): 19–34. http://dx.doi.org/10.1016/0301-9322(90)90034-G.

Chialvo, A.A. and Debenedetti, P.G. 1990. On the Use of the Verlet Neighbor List in Molecular Dynamics. *Comput. Phys. Commun.* **60** (2): 215–224. http://dx.doi.org/10.1016/0010-4655(90)90007-N.

Crowe, C.T., Schwarzkopf, J.D., Sommerfeld, M., et al. 2011. *Multiphase Flows with Droplets and Particles*. Boca Raton, Florida: CRC Press.

Fritsching, U. 2004. *Spray Simulation: Modeling and Numerical Simulation of Sprayforming metals*. Cambridge, UK: Cambridge University Press.

Haider, A. and Levenspiel, O. 1989. Drag Coefficient and Terminal Velocity of Spherical and Nonspherical Particles. *Powder Technol.* **58** (1): 63–70. http://dx.doi.org/10.1016/0032-5910(89)80008-7.

Hatch, A. and Kamholz, A. 2001. A Ferrofluidic Magnetic Micropump. *J. Microelectromech. S.* **10** (2): 215–221. http://dx.doi.org/10.1109/84.925748.

Jordan, A., Scholz, R. and Wust, P. 1999. Magnetic Fluid Hyperthermia (MFH): Cancer Treatment with AC Magnetic Field Induced Excitation of Biocompatible Superparamagnetic Nanoparticles. *J. Magn. Magn. Mater.* **201** (1–3): 413–419. http://dx.doi.org/10.1016/S0304-8853(99)00088-8.

Kim, I., Elghobashi, S. and Sirignano, W.A. 1998. On the Equation for Spherical-Particle Motion: Effect of Reynolds and Acceleration Numbers. *J. Fluid Mech.* **367** (1): 221–253. http://dx.doi.org/10.1017/S0022112098001657.

Liu, B. and Pui, D. 1974. Electrical Neutralization of Aerosols. *J. Aerosol Sci.* **5** (5): 465–472. http://dx.doi.org/10.1016/0021-8502(74)90086-X.

Maxey, M.R. and Riley, J.J. 1983. Equation of Motion for a Small Rigid Sphere in a Nonuniform Flow. *Phys. Fluids* **26:** 883–889. http://dx.doi.org/10.1063/1.864230.

Mei, R. 1994. Flow Due to an Oscillating Sphere and an Expression for Unsteady Drag on the Sphere at Finite Reynolds Number. *J. Fluid Mech.* **270** (July): 133–174. http://dx.doi.org/10.1017/S0022112094004222.

Mei, R. and Adrian, R. 1992. Flow Past a Sphere with an Oscillation in the Free-Stream Velocity and Unsteady Drag at Finite Reynolds Number. *J. Fluid Mech.* **237** (April): 323–341. http://dx.doi.org/10.1017/S0022112092003434.

Oden, J. and Pires, E. 1984. Algorithms and Numerical Results for Finite Element Approximations of Contact Problems with Non-Classical Friction Laws. *Comput. Struct.* **19** (1–2): 137–147. http://dx.doi.org/10.1016/0045-7949(84)90212-8.

Odenbach, S. 2003. Ferrofluids—Magnetically Controlled Suspensions. *Colloid. Surface. A* **217** (1–3): 171–178. http://dx.doi.org/10.1016/S0927-7757(02)00573-3.

Peasley, K.W. 1996. Destruction of Human Immunodeficiency-Infected Cells by Ferrofluid Particles Manipulated by an External Magnetic Field: Mechanical Disruption and Selective Introduction of cytotoxic or antiretroviral substances into target cells. *Med. Hypotheses* **46** (1): 5–12. http://dx.doi.org/10.1016/S0306-9877(96)90226-1.

Pöschel, T. and Schwager, T. 2005. *Computational Granular Dynamics: Models and Algorithms*. Berlin, Germany: Springer.

Sinha, A., Ganguly, R., De, A.K., et al. 2007. Single Magnetic Particle Dynamics in a Microchannel. *Phys. Fluids* **19** (11): 117102-1–117102-5. http://dx.doi.org/10.1063/1.2780191.

US Department of Transportation (DOT). 2014. Pipeline and Hazardous Materials Safety Administration, http://phmsa.dot.gov/pipeline/.

Wriggers, P. and Zavarise, G. 2002. *Computational Contact Mechanics*. Berlin, Germany: Springer.

Zohdi, T.I. 2007. *An Introduction to Modeling and Simulation of Particulate Flows*. Philadelphia, Pennsylvania: Society for Industrial and Applied Mathematics.

Zohdi, T. 2010. On the Dynamics of Charged Electromagnetic Particulate Jets. *Arch. Comput. Method. E.* **17** (2): 109–135. http://dx.doi.org/10.1007/s11831-010-9044-3.

Debanjan Mukherjee is a post-doctoral research scholar at the Department of Mechanical Engineering at the University of California, Berkeley. His research interests include discrete-element methods, finite-element methods, granular flows and granular dynamics, multiphase and particle-laden flows, numerical methods for fluid/particle interaction, and modeling of biological flows. Mukherjee holds master's and PhD degrees in mechanical engineering from the University of California, Berkeley, and earned a bachelor's degree in ocean engineering from the Indian Institute of Technology, Madras, India.

Zeyad A. Zaky is a PhD degree student in mechanical engineering at the University of California, Berkeley. His research project focuses on discrete-element methods, namely particle-embedded flows. Zaky holds bachelor's and master's degrees in mechanical engineering from the University of California, Los Angeles.

Tarek I. Zohdi is a professor of mechanical engineering; Chair of the Designated Emphasis Program in Computational and Data Science and Engineering; and Chancellor's Professor at the University of California, Berkeley. His main research interests are in micromechanical-material design, particulate flow, and the mechanics of high-strength fabric, with emphasis on computational approaches for advanced manufacturing and nonconvex multiscale/multiphysics inverse problems. Zohdi has published more than 120 archival refereed-journal papers and five books. He holds a PhD degree in computational and applied mathematics from the University of Texas at Austin and a Habilitation in mechanics from the Gottfried Leibniz University of Hannover, Germany.

Amgad Salama is currently an associate researcher at the Computational Transport Phenomena Laboratory at King Abdullah University of Sciences and Technology, Saudi Arabia. Previously, he worked as a research fellow at Kyushu University, Japan, for 2 years and as an assistant professor at the Department of Environmental Engineering at Konkuk University, South Korea, for more than 2 years. Salama's research work is interdisciplinary, focusing mainly on areas related to heat transfer and fluid flows in mechanical systems as well as to transport phenomena in porous media. He holds bachelor's and master's degrees in mechanical engineering from El Menoufia University and Cairo University, Egypt, respectively, and a PhD degree in environmental engineering from Carleton University, Canada.

Shuyu Sun is currently the principal investigator and head of the Computational Transport Phenomena Laboratory at King Abdullah University of Science and Technology and a codirector of the Center for Subsurface Imaging and Fluid Modeling consortium at King Abdullah University. He is a founding faculty member jointly appointed by the program of Earth Sciences and Engineering and the program of Applied Mathematics and Computational Science, and is an associate professor. Sun also holds a number of adjunct faculty positions internationally, including adjunct professorships at Xi'an Jiao Tong University and China University of Petroleum at Beijing, and an adjunct associate professorship at Clemson University. Before joining King Abdullah University, he served as an assistant professor of mathematical sciences at Clemson University. In addition to numerous conference papers and technical reports, Sun has published more than 90 refereed-journal articles. He currently serves as an editor, guest editor, associate editor, or editorial board member for seven international refereed journals in his field. Sun is also a licensed professional engineer in Texas. He is a member of SPE and participated in the SPE Petroleum Engineering Certification Program. Sun serves as the faculty adviser of King Abdullah University's SPE Student Chapter, and recently he received a certification from SPE recognizing him as "serving exceptionally well as Student Chapter Faculty Adviser." He earned a PhD degree in computational and applied mathematics from the University of Texas at Austin, and a Doctor of Engineering degree in chemical engineering from Tianjin University.